JCTC Journal of Chemical Theory and Computation

Article

pubs.acs.org/JCTC

Toward Fast and Accurate Evaluation of Charge On-Site Energies and Transfer Integrals in Supramolecular Architectures Using Linear Constrained Density Functional Theory (CDFT)-Based Methods

Laura E. Ratcliff,*[,†,‡,⊥] Luca Grisanti,*[,¶,§] Luigi Genovese,[†,‡] Thierry Deutsch,[†,‡] Tobias Neumann,[∥] Denis Danilov,[∥] Wolfgang Wenzel,[∥] David Beljonne,[¶] and Jérôme Cornil*[,¶]

[†]Université Grenoble Alpes, INAC-SP2M, L_Sim, F-38000 Grenoble, France

[‡]CEA, INAC-SP2M, L_Sim, F-38000 Grenoble, France

[¶]Laboratory for Chemistry of Novel Materials, University of Mons, Place du Parc 20, B-7000 Mons, Belgium

[§]The Abdus Salam International Centre for Theoretical Physics (ICTP), Strada Costiera 11, I-34151 Trieste, Italy

[∥]Institute of Nanotechnology, Karlsruhe Institute of Technology (KIT), 76344 Eggenstein-Leopoldshafen, Germany

Supporting Information

ABSTRACT: A fast and accurate scheme has been developed to evaluate two key molecular parameters (on-site energies and transfer integrals) that govern charge transport in organic supramolecular architecture devices. The scheme is based on a constrained density functional theory (CDFT) approach implemented in the linear-scaling BigDFT code that exploits a wavelet basis set. The method has been applied to model disordered structures generated by force-field simulations. The role of the environment on the transport parameters has been taken into account by building large clusters around the active molecules involved in the charge transfer.

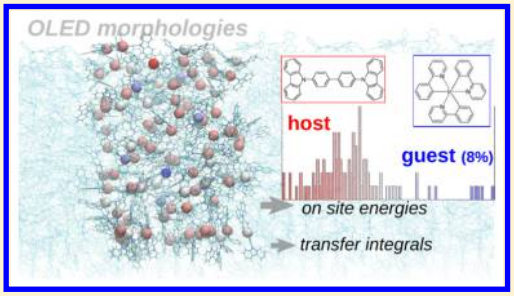

1. INTRODUCTION

In molecular materials, modeling charge transport processes requires a series of steps that interface different computational approaches, in such a way as to provide a picture that scales from the microscopic (atomistic) scale to macroscopic material properties.[1−4] In most atomistic approaches, the typical steps involve:

(1) *in silico* formation of the material morphology (e.g., using molecular mechanics/molecular dynamics (MM/MD) methods);
(2) the evaluation of microscopic electronic parameters (i.e., on site energies and transfer integrals) on the basis of the generated structure (in most cases, quantum-chemical approaches are applied at this level, depending on the size of the system the level of theory used ranges from semiempirical to DFT and more-sophisticated approaches); and
(3) a numerical model to describe the propagation of the charge and macroscopic properties such as charge mobility based on the electronic parameters inferred at stage 2.

The interconnection of the different steps is of major importance to develop truly multiscale theoretical workflows.[1−3]

Most modern transport theories that are relevant for organic molecular solids refer to the concept of a polaron as a charged state in which the degree of charge localization is dependent on the magnitude of the electron−phonon couplings and the amount of disorder.[5−8] The transport models all share the common characteristic that they rely on two key ingredients, namely, the charge on-site energies and transfer integrals, whose direct estimation requires methods able to *prepare* diabatic states, such as constrained density functional theory (CDFT)[9−13] or fragment orbital methods.[14] Moreover, since the molecular units are embedded in the material structure, a realistic description of the influence of the environment must be achieved to provide a reliable and complete picture. Improving the accuracy of the calculated parameters by refining the existing computational tools or proposing new approaches is of utmost importance for the field; since disordered structures contain many different pairs of interacting molecules, finding ways to accelerate the time required for computing parameters is another great challenge. Among the computational tools developed, DFT-based techniques still remain the most popular. In this context, we describe here a new fast and accurate theoretical approach for evaluating on-site energies and charge-transfer integrals on the basis of a CDFT method implemented in the linear-scaling BigDFT code, which uses a wavelet basis set. This theoretical methodology has then been applied to a supramolecular architecture based on representative materials for the organic light-emitting diode (OLED) technology, i.e., a host transport matrix doped with optically

Received: January 21, 2015
Published: April 9, 2015

DOI: 10.1021/acs.jctc.5b00057
J. Chem. Theory Comput. 2015, 11, 2077−2086

active centers (*guest*) where holes and electrons eventually recombine to produce excitations that can decay radiatively. If the recombination occurs on the host, the produced excitation will first have to travel through the material before ideally getting trapped in the guest center, which is responsible for the emission. Large quantum yields are typically obtained by employing Ir-based complexes as guests to exploit both singlet and triplet excitons for light emission via a phosphorescence signal.[15−18]

The large heterogeneity of such host−guest structures makes them attractive: (i) to investigate at a fundamental level the way the *energy landscape* for charge carriers is affected when introducing guest molecules in the host matrix; and (ii) to test our new scheme combining high accuracy and high speed to evaluate the transport parameters. In this work, the structures are built with the host molecule, 4,4′-*N*,*N*′-dicarbazole-biphenyl (CBP) and combined with the tris(2-phenylpyridine) iridium, $Ir(ppy)_3$, iridium triplet emitter as the guest (see Figure 1).

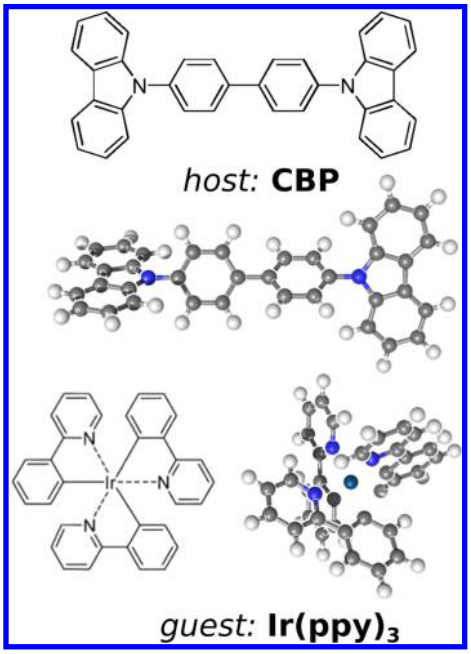

Figure 1. Structures of the host (top and middle) and guest molecules (bottom) used for the simulations, as well as their three-dimensional structures.

2. THEORY AND COMPUTATIONAL METHODOLOGY

At room temperature, charge transport in disordered materials mostly operates in a hopping regime in which the charges hop from molecule to molecule to give rise to an electrical current.[6] In this framework, from a purely electronic point of view, the two parameters playing a crucial role are the on-site energies (the total energy associated with the charge occupation of the molecular site *r*, namely, the ionization potential (IP) for holes and electron affinity (EA) for electrons in the *solid state*) and the transfer integrals (describing the hopping probability between sites *r* and *s*). On one hand, the IP and EA values are often computed in a one-electron picture by relying on Koopmans' theorem from the highest occupied molecular orbital (HOMO) and lowest unoccupied molecular orbital (LUMO) energies, respectively; we stress that the use of the CDFT approach will allow us to go beyond this one-electron approximation and obtain the corresponding values from differences between total energies. On the other hand, the transfer integrals are most often computed between orthogonalized one-electron wave functions (HOMOs of the individual units for holes and LUMOs for electrons).

2.1. Fragment Approach in BigDFT. The BigDFT[19] electronic structure code employs a Daubechies wavelet basis set, taking advantage of the orthogonality, compact support and smoothness of such a basis to solve the Kohn−Sham (KS) equations to a high, controllable precision. Furthermore, BigDFT has been explicitly designed to run efficiently on massively parallel architectures, so that relatively large system sizes can be treated (several hundreds of atoms). Nonetheless, its applicability is limited by the asymptotic cubic scaling, with respect to the number of atoms, which is common to standard DFT implementations. To this end, a new approach has recently been implemented in BigDFT, using a minimal set of localized "support functions" represented in this underlying wavelet basis set, in other terms using an adaptively contracted wavelet basis set. These support functions are optimized *in situ* and thus provide an optimal basis for a given system, at the same time reducing the scaling of BigDFT; when combined with the appropriate sparse matrix algebra, this leads to a linear scaling behavior with the number of atoms. This approach, which has been described elsewhere,[20] facilitates calculations on thousands of atoms at moderate computational cost while retaining the systematically controllable accuracy of the underlying wavelet basis set. Furthermore, the support function approach can easily be adapted for fragment calculations, wherein a given system is divided into groups of atoms; in our case, these groups or "fragments" correspond to the individual molecules. The support functions are fully optimized for the isolated fragments and are then used as a fixed basis for the full system, so that only the density has to be recalculated self-consistently. Such a procedure is not only substantially less expensive than a full calculation wherein the support functions are optimized, but also provides a natural way of calculating the transfer integrals and on-site energies. This approach is similar to the fragment orbital method applied in ADF and elsewhere.[21−23] However, rather than using the KS orbitals from the fragments as a basis, e.g., the HOMO of each fragment, we instead use the support functions from each fragment. Since the support functions remain fixed, the fragment KS orbitals can of course still be expressed in this basis; however, the use of support functions affords additional flexibility for the calculation of the density.

Since we are interested in our case study in calculating transfer integrals mostly between two identical molecules with different orientations, the support function approach has yet another advantage. Indeed, an interpolation scheme has been developed in BigDFT, allowing for the support functions to be fully optimized for an example, or "template" molecule, and then rotated and shifted across the wavelet grid for other orientations of the molecule. This approach, which is described elsewhere,[24] has been shown to have a negligible impact on the accuracy of the basis and therefore allows for a consistent treatment of molecules across the structure. In particular, this implies that the *sign* of the transfer integral will be calculated correctly between identical fragments, as there will be no ambiguous phase. Furthermore, in a system involving a large number of identical fragment types such as the systems involved in this work, only a small number of template

DOI: 10.1021/acs.jctc.5b00057
J. Chem. Theory Comput. 2015, 11, 2077−2086

calculations (one per fragment type) are required, which can further reduce the computational cost.

An additional step must be performed in the calculation of transfer integrals and on-site energies in order to correctly account for the nonorthogonality of the new basis within the fragment approach. This is due to the fact that, while the KS orbitals are correctly orthogonal for the isolated fragments, they are generally nonorthogonal between fragments. Therefore, the KS orbitals of the complete system are orthogonalized before the transfer integrals and on-site energies are calculated. This can be done just for the levels of interest, e.g., only the HOMO levels of the different fragments, but we instead choose to perform the orthogonalization between all orbitals in the occupied manifold of the fragments plus the unoccupied levels of interest. The differences between the two approaches for this system are small, but we have found that the latter approach is generally more stable and allows for a consistent treatment of the electron and hole quantities, including any degenerate states. We have also verified that there is no detrimental effect on the spread of the KS orbitals due to the orthogonalization, instead they remain strongly localized on their original molecules.

It should also be stressed that the optimization procedure used to generate the support functions for the isolated fragments is based on energy minimization, and as such, only the occupied KS orbitals are guaranteed to be accurately represented. For calculations where we are interested in electron transport, care must be taken to ensure that the LUMO is also well represented in the support function basis. This can be achieved by explicitly including a few unoccupied states in the optimization procedure, for which the direct minimization method for density kernel optimization must be employed (see ref 20 for further details).

2.2. On-Site Energies with Constrained DFT. The fragment approach discussed above provides a good initial approximation for the on-site energies. However, there are some limitations essentially linked to the use of a one-electron picture, further implying that the complete system systematically remains neutral. One way of improving upon this approximation involves the use of constrained DFT, wherein a Lagrange multiplier term is added to the KS energy functional, thereby enforcing an additional constraint on the electronic density. In our case, this will take the form of a localization constraint for the net charge introduced in the system. The principles and various applications of CDFT have been covered in many recent works,[9,10,21,25−29] so, here, we will summarize only the key points. The constraint term involves two key components: a weight function ($w_c(\mathbf{r})$) and a Lagrange multiplier (V_c). The former is used to specify the region of space over which the charge is constrained and is thus defined by the user and held fixed during the calculation, while the correct value of the latter must be found during the calculation using a given optimization scheme. Using these two quantities, the functional to be minimized can be written as

$$W[\rho, V_c] = E_{KS}[\rho] + V_c\left(\int w_c(\mathbf{r})\rho(\mathbf{r})\,d\mathbf{r} - N_c\right) \quad (1)$$

where $E_{KS}[\rho]$ is the original KS energy functional, ρ is the electronic charge density, and N_c is the required charge within the specified region. The correct value of V_c is found using Newton's method, by calculating the second derivative using a finite difference approach. In practice, this is rewritten as a matrix equation, so that the weight matrix can be directly defined from the support functions using a Löwdin-like definition to associate a given fragment with a region of space. This choice of the Löwdin weight function over other options is motivated both by the ease with which it is defined in our approach and the low computational overhead. Furthermore, we have found it to give accurate results for systems such as this one, where the fragments are well-defined and separated, in agreement with other studies where the differences with other weight functions such as the Becke weight function are very small at larger distances.[10,30]

The on-site energies for holes (electrons) of a molecule in a given environment are extracted using CDFT as follows. First, a reference neutral calculation is performed to obtain the total energy for the molecule in its environment. Second, a calculation is performed with an overall charge of ±1, using CDFT to force the excess charge to remain on the molecule of interest. The on-site energies are then defined as

$$E^{hole} = E_{tot}^{+1} - E_{tot}^{0} \quad (2)$$

$$E^{electron} = E_{tot}^{-1} - E_{tot}^{0} \quad (3)$$

In order to include environmental effects when estimating the transport parameters, we systematically form a cluster made of the nearest neighbors around each molecule (correctly taking into account the surface boundary conditions) to calculate the on-site energies, both in the fragment approach and using CDFT. It is worth stressing that the cluster built around the central charged molecule in CDFT grasps only a fraction of the electronic polarization, which is a long-range effect. However, this approach is validated by the fact that the relative energy between two molecular sites is the only quantity appearing in transfer rates within a hopping regime in disordered structures.[8]

2.3. Transfer Integrals. Transfer integrals are typically calculated between pairs (dimers) of neutral molecules (J_{ij}^{d}); however, in order to account for the environmental effects, here, we also calculate the transfer integrals in the clusters built with the nearest neighbor (J_{ij}^{C}). Since the actual calculation of the transfer integrals is much less time-consuming, compared to the other components of DFT calculations, it is much less expensive to estimate the on-site energies and transfer integrals in the clusters simultaneously, compared to performing additional calculations for pairs of molecules, which, despite being relatively fast, would significantly add to the computational costs, given the large number of calculations required. However, such an approach could add some asymmetry to the transfer integrals, i.e., $J_{ij}^{C} \neq J_{ji}^{C}$, as the nearest-neighbor cluster of i will not be the same as that of j. In order to be more rigorous, one should calculate the transfer integrals in clusters of the nearest neighbors of both i and j. Although the results for such biclusters (J_{ij}^{bC}) would be symmetric, the computational overheads would again increase. Therefore, we have continued to use the nearest-neighbor clusters, averaging the results for J_{ij} and J_{ji}:

$$\bar{J}_{ij}^{C} = \frac{J_{ij}^{C} + J_{ji}^{C}}{2}$$

Transfer integrals were calculated for a limited number of biclusters in order to validate this approach; it was found that the differences between such averaged values and the bicluster results were close to negligible. The Supporting Information (especially Figure SI 3), shows further details about our computational approach to access the transfer integrals.

DOI: 10.1021/acs.jctc.5b00057
J. Chem. Theory Comput. 2015, 11, 2077−2086

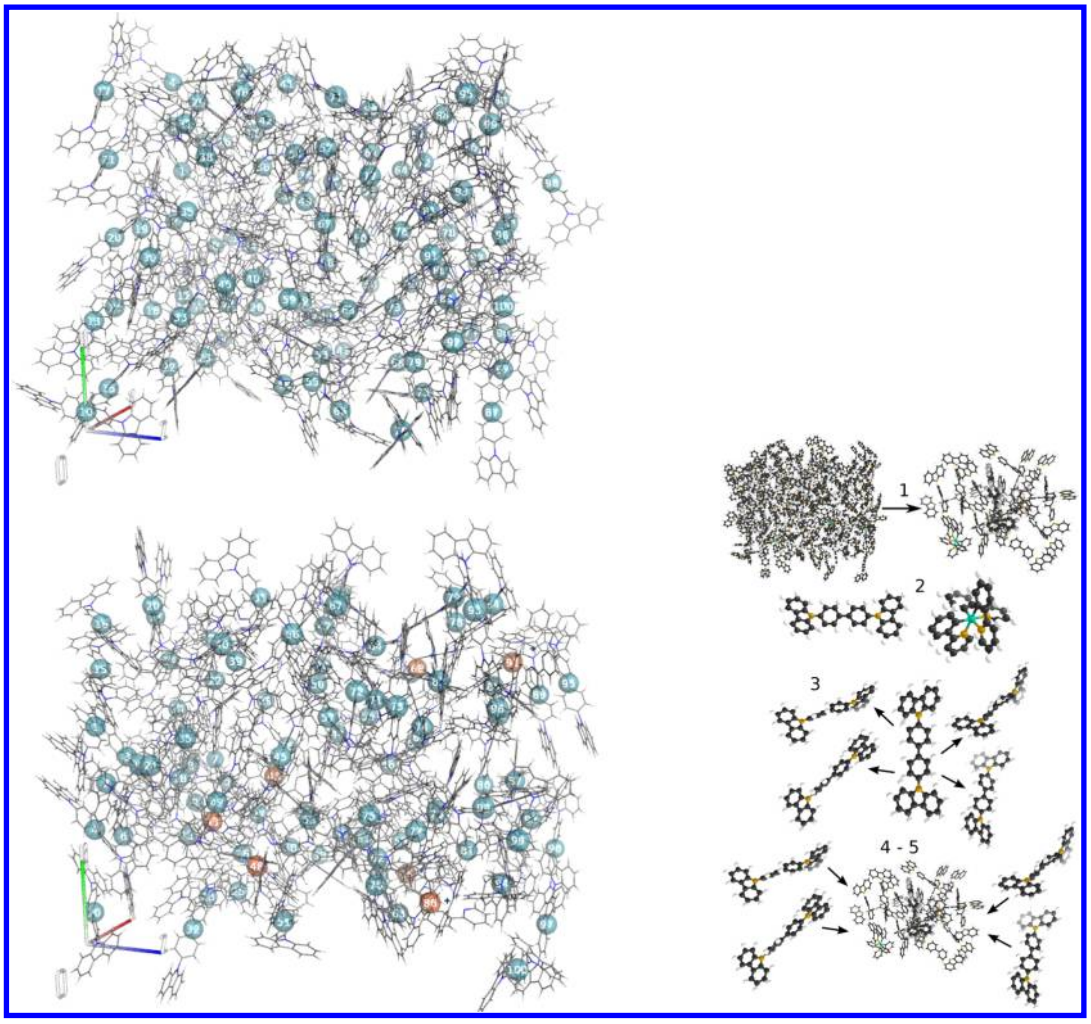

Figure 2. (Left) Morphologies generated for the pure host matrix (top) and the host−guest system (bottom); we display the chemical structures and their respective centers of mass (blue indicates the host molecule, and orange red indicates the guest molecule). (Right) Schematic illustration of the procedure for calculating the transfer integrals and on-site energies, taking into account the environmental effects.

2.4. Method. Therefore, the overall procedure to extract both transfer integrals and on-site energies for the host−guest system involves five steps, which are decribed as follows and illustrated in the righthand side of Figure 2:

(1) For each molecule in the system, a cluster of its nearest neighbors is formed, taking into account the surface boundary conditions.
(2) The support functions are fully optimized for each of the template molecule types; care is taken to ensure the LUMO is well-represented in each case.
(3) The support functions from the template molecules are reformatted for different orientations and positions within each cluster of nearest neighbors. In practice, this step is performed automatically by BigDFT at the start of the cluster calculations.
(4) The density is self-consistently calculated in the nearest neighbor clusters in the basis of the reformatted support functions, following which the transfer integrals and on-site energies are calculated using the orthogonalized fragment orbitals.
(5) Constrained DFT calculations are performed for positive and negative charges constrained on the central molecule of the cluster. The corresponding total energies from these and the calculations in step 4 are then used to calculate the on-site energies.

2.5. Computational Details. There are different methods to produce thin films in organic electronic devices. While solution-based processing is relatively inexpensive and large surfaces can be created with roll-to-roll processes, the devices suffer from many defects and fast degradation. Deposition via vacuum physical vapor deposition (PVD) is more difficult but produces devices with higher stability and longer lifetimes. Ultrastable properties of thin films prepared by PVD have also been observed for several organic glasses.[31,32] Numerical simulations[33] show that the exceptional stability can be explained by an enhanced mobility of the deposited molecules on the surface of the film in comparison to the low mobility of molecules in the bulk when they are surrounded by other particles. Therefore, the molecules on the surface of the film are able to explore a larger part of the configuration space and find an energetically favorable position.

The morphologies used here were created by a single molecule deposition protocol[3] that mimicked a PVD process. In order to model the characteristics of the real deposition process, which leads to ultrastable organic glasses, the computational protocol includes the following features, as illustrated in Figure 3. A Metropolis Monte Carlo (MC)

DOI: 10.1021/acs.jctc.5b00057
J. Chem. Theory Comput. 2015, 11, 2077−2086

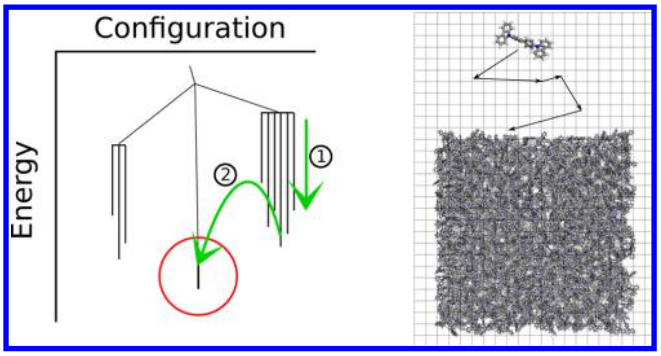

Figure 3. Efficient morphology generation by single molecule deposition. (Left) Metropolis Monte Carlo in combination with repeated simulated annealing is applied to reach minima in energy (denoted by "①") for hopping between different local minima in the configuration space (denoted by "②"). (Right) During the deposition of a single molecule, the molecules in the substrate are kept fixed, which allows for the precalculation of the interaction energies between the substrate and the new molecule on points of a grid. Linear interpolation is applied for a very fast evaluation of the energy over the course of the deposition.

approach,[34] combined with the simulated annealing method,[35] is used to find a configuration in a local minimum in energy for a deposited molecule on the film surface. The basin hopping method[36−38] is applied by repeated simulated annealing to find the global minimum of the energy by hopping between the local minima computed by MC.

The large mobility of the molecules on the film surface helps to find an energetically optimized configuration and allows for an additional approximation: after the deposition, the molecules are kept frozen. This approximation can be exploited for computationally efficient evaluation of the intermolecular interactions. During the deposition of a single molecule onto an already existing film, the molecules in the substrate are kept fixed, inducing a static force field. The interaction energy between the new molecule and the substrate can then be precalculated on points of a three-dimensional (3D) grid. During each Monte Carlo step of the deposition process, the interaction energy between the new molecule above the surface and the substrate is calculated by linear interpolation between the grid points, as illustrated in Figure 3.

The following settings were used in the morphology simulations: each new molecule was added at a distance of 5 nm above the surface of the film and then deposited using 10 simulated annealing cycles consisting of 20 000 MC steps each, cooling from 1000 K to 300 K. Periodic boundary conditions in (x,y) directions were applied. Because of the rigidity of the molecules considered in this work, internal movement (angle bending, torsion, and bond stretching) was neglected, which may lead to an underestimation of the energy difference, in comparison to conformations where angle bending and bond stretching is permitted. The intermolecular interaction was modeled by a force field approach using Coulomb electrostatics and a standard Lennard-Jones potential for van der Waals attraction and Pauli repulsion. Unit cells with a size of of 40 Å × 40 Å and containing 100 molecules were obtained for the pure host (100% CBP) and for the host−guest structure (92% CBP and 8% $Ir(ppy)_3$), as displayed on the left side of Figure 2. For each molecule, all of the nearest neighbors with a center-to-center distance of <15 Å were included in the clusters to account for the environment.

The BigDFT calculations were performed using the local density approximation (LDA) exchange-correlation functional[39] and HGH pseudo-potentials.[40] Free-boundary conditions were applied, as the correct surface boundary conditions were already accounted for when forming the clusters of nearest neighbors. The grid spacing and other wavelet basis set parameters were selected such that the resulting accuracy for the template calculations was of the order of 1 meV/atom. We used 1 support function per hydrogen atom, 4 per carbon or

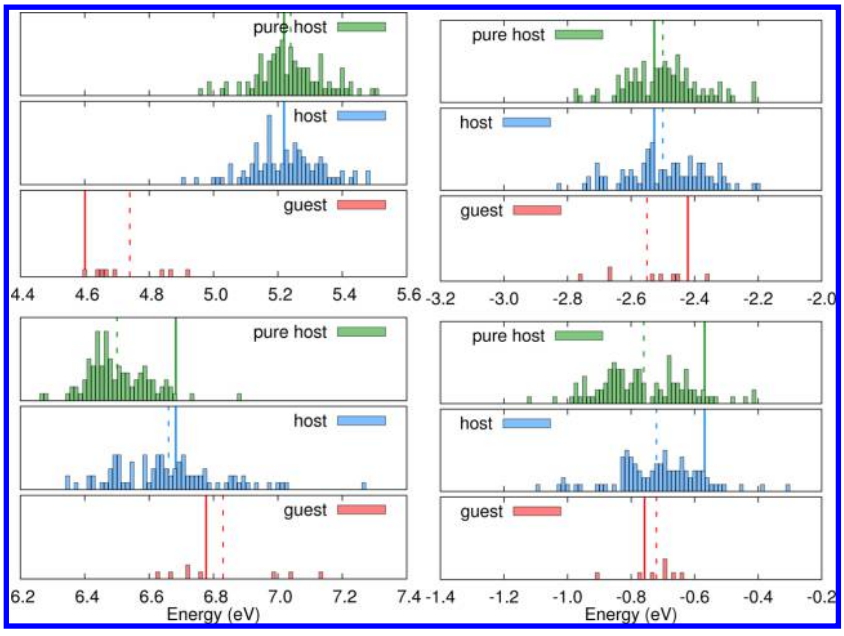

Figure 4. Comparison between the on-site energy distributions for holes (left) and electrons (right) when considering the fragment approach (top) versus the CDFT cluster calculations (bottom). The solid vertical lines represent the values for the isolated molecules obtained from HOMO or LUMO energy levels (top left and right, respectively) and from the total energies of the neutral and charged systems (bottom left and right, respectively). The broken vertical lines correspond to the average values.

DOI: 10.1021/acs.jctc.5b00057
J. Chem. Theory Comput. 2015, 11, 2077−2086

Table 1. On-Site Energies (with Average Values and Standard Deviations in Clusters) for Holes and Electrons Calculated with the Different Methods and Levels of Approximation, Compared to Available Experimental Data (Bottom Lines)

			Pure Host		Host−Guest			
			Host		Host		Guest	
			h	*e*	*h*	*e*	*h*	*e*
calculated, 1 *e*								
	isolated	$E \equiv \mp\varepsilon^{H,L}$	5.22	−2.52	5.22[a]	−2.52[a]	4.60	−2.42
	fragment	$\langle E\rangle \equiv \langle \mp\varepsilon^{H,L}_{frag}\rangle$	5.24	−2.50	5.22	−2.50	4.74	−2.55
		σ_E	0.11	0.12	0.11	0.13	0.11	0.12
calculated, all *e*								
	isolated	$E \equiv E^{+1,-1} - E^0$	6.68	−0.57	6.68[a]	−0.57[a]	6.78	−0.76
	isolated, opt[b]	$E \equiv E^{+1,-1} - E^0$	6.65	−0.88	6.65[a]	−0.88[a]	6.65	−0.93
	isolated, SD[c]	$E \equiv E^{+1,-1} - E^0$	6.56	−0.92	6.56[a]	−0.92[a]	6.30	−1.00
	CDFT	$\langle E\rangle \equiv \langle E^{+1,-1}_{tot} - E^0_{tot}\rangle$	6.50	−0.76	6.66	−0.72	6.83	−0.72
		σ_E	0.10	0.14	0.17	0.14	0.18	0.08
experiment								
	ref 42	UPS (film)	6.0	2.9[d]				
	ref 43	UPS	6.8					
	ref 17	(film)	6.0				5.4[e]	
	ref 44	UPS, CV (film)					5.10[e]	
	ref 15	(ref 15 and information therein)					5.2	2.8[e]
	ref 45	UPS	6.1	2.0[d]				

[a]Energies for isolated molecules are the same in mixed phases versus pure phases. [b]Using the fully optimized basis. [c]Spin polarized density calculations using the fully optimized basis. [d]Estimated by adding the optical gap[42] or the edge-to-edge gap.[45] [e]Relative to the pure guest.

nitrogen atom, and 16 per iridium atom with localization radii of 4.76 Å. As previously mentioned, the direct minimization scheme was used for the density kernel optimization, including 1 unoccupied state in the optimization procedure for the template calculations. Furthermore, the template calculations were performed using a denser wavelet grid to ensure the accuracy of the reformatting procedure for rotating the support functions. Test calculations performed with BigDFT in the fragment approach were also validated against that implemented in ADF,[41] for selected dimer pairs and other model systems. A good agreement was found between the two codes when a converged basis set was used in ADF (see Table SI 1 in the Supporting Information).

3. RESULTS AND DISCUSSION

The crudest approximation for evaluating the on-site energies in a disordered structure would be to neglect the environment and assume that all molecules (of the same species) have the same energies. Such values could be inferred from single molecules using a one-electron picture (Koopman's approximation) or at the all-electron level (as the energy difference between the total energy of the neutral and charged systems), see straight lines in Figure 4. As a refinement, the impact of the surrounding environment can be introduced at two levels: by adopting the fragment approach while still using a single orbital description, or by going to constrained DFT at the multielectronic level, as described in Section 2.2. The results obtained for the host (in the pure phase as well as in the host−guest structure) and guest molecules, adopting these two different approaches, are summarized in Table 1 and Figure 4.

The introduction of a structured electrostatic landscape by the environment translates into two main effects: a distribution of the on-site energies and an overall shift of the average energies. The width of the distribution due to the electrostatic disorder induced by the different molecular orientations is already accounted for by the fragment approach, although to a lesser extent, compared to CDFT in the case of the host−guest structure (see Table 1). However, the fragment approach is not able to produce relevant shifts, with respect to the isolated molecule reference, especially for the host. Different trends for the on-site energy shifts are observed when comparing the fragment approach and CDFT, because of the fact that the latter accounts for solid-state polarization effects induced by the presence of an excess charge.

The isolated all-electron hole energies are 6.68 eV for CBP and 6.78 eV for the iridium complex, while the CDFT-calculated average hole energies slightly differ: 6.50 and 6.66 eV for CBP (in the pure and host−guest morphology, respectively) and 6.83 eV for the iridium complex. Although solid-state UPS data are available[17,42−44] (see also Table 1), these can hardly be compared to the results of our cluster approach that only accounts for a small portion of the solid-state electronic polarization effects. Nonetheless, it is useful to consider the potential sources of error in our calculations. There is a small error introduced due to the use of a fixed support function basis (generated for the neutral structure), compared to a basis that is fully optimized for each charge state. It is slightly larger for the guest molecule but, nonetheless, remains modest: ∼0.1 eV in the worst case (see Table 1). This difference is more significant for electrons (up to 0.3 eV), so that, in the future, one might consider including further unoccupied states in the optimization procedure other than the LUMO in the hope of decreasing this error. For the hole calculations, a more important source of error might be the choice of exchange-correlation functional. In order to assess the impact of the LDA choice, calculations were also performed for the isolated molecules using B3LYP in the full wavelet basis (i.e., no localized support functions), for which the results are 6.90 and 6.85 eV. Further calculations would have to be performed to determine whether B3LYP would significantly affect the results when the environment is included, although it is reasonable to assume the trends would remain similar to the LDA results.

DOI: 10.1021/acs.jctc.5b00057
J. Chem. Theory Comput. 2015, 11, 2077−2086

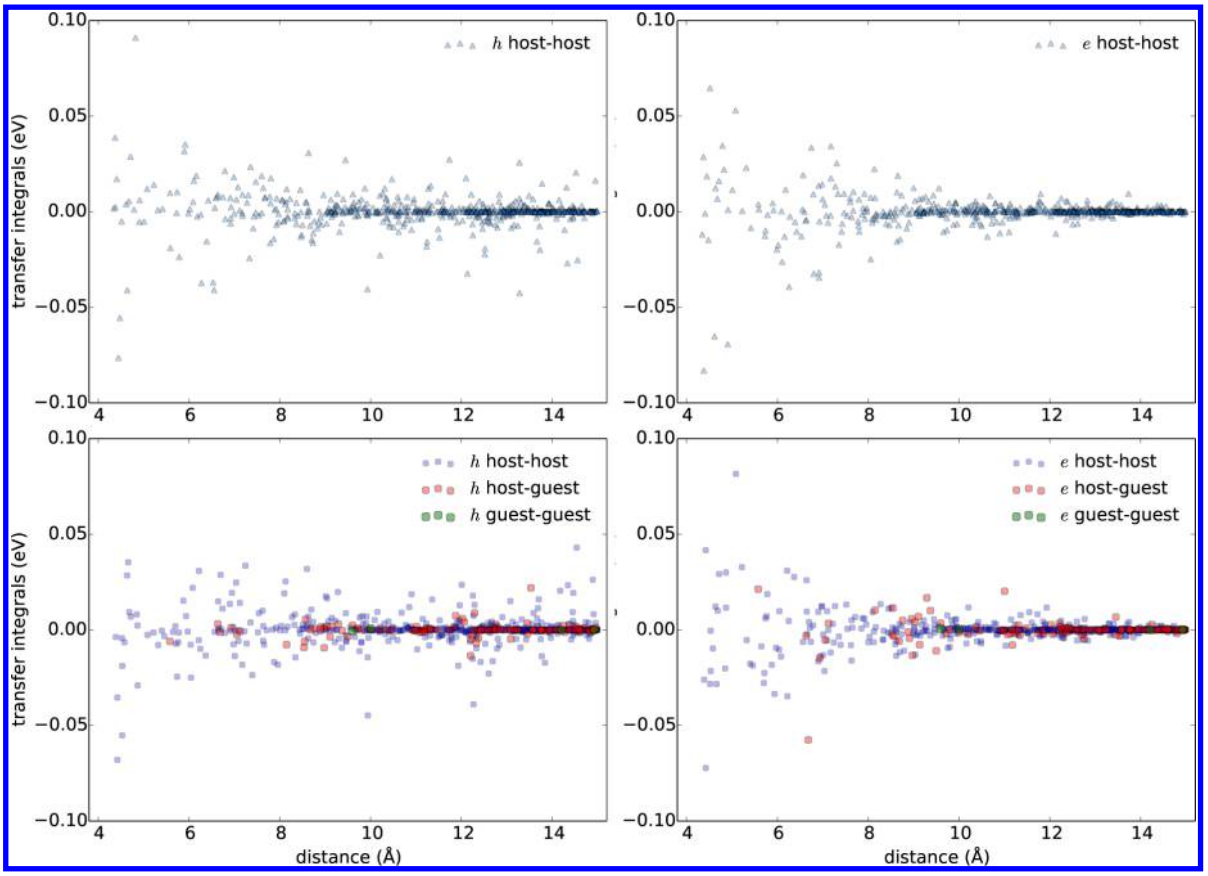

Figure 5. Transfer integral (J_{ij}^{C}, see text) as a function of the separation between the centers of mass for holes (left) and electrons (right), in the pure host (top) and host−guest structure (bottom).

All calculations were performed in the restricted formalism, i.e., orbitals of different spin were not treated independently, rather each orbital was fixed at either double or single occupation to preserve only the correct average spin with no overall polarization. This was necessary to reduce the computational cost, since, in order to maintain the same accuracy for spin-polarized as for restricted calculations, an independent set of support functions is needed for each spin state, thereby doubling the cost of the calculations. In order to determine the impact of this neglect, we performed some tests on the isolated units: the inclusion of spin polarization has the effect of decreasing the calculated IP for the guest molecule by ∼0.4 eV, while the effect is much less important for the host molecule (reduction by ∼0.1 eV). The values in the fully optimized basis are 6.56 eV and 6.30 eV for the host and guest, respectively. (See Table 1 for all of the results.)

In the host−guest structure, the CDFT calculations predict the average on-site energy for holes to be higher by ∼0.1 eV for the iridium complex, compared to the host CBP, in contrast with experimental data pointing to an energetically unfavorable hole transfer from the guest to the host. Ishihara et al.[17] suggested that holes are directly injected into the guest from the indium tin oxide (ITO), and that transfer from the guest to host molecules is thermally activated (barrier of 0.6 eV). Unexpectedly, and probably because of an error compensation, this trend is recovered by the simpler fragment method, with a barrier of 0.5−0.6 eV. As discussed above, the discrepancy in the CDFT results could be mainly attributed to the neglect of spin polarization, although it should also be noted that the experimental offset is estimated from the values obtained for the pure host and guest molecules and that the actual value in the blend might be different.[17,45] Interestingly, the CDFT results obtained for holes display a much larger overlap between the distribution of site energies calculated for the host versus guest molecules, compared to the fragment approach; this opens possible hole transfer pathways from the host to the guest, as evidenced experimentally. The shift of the average on-site energy of the host going from the pure phases to the blend further amplifies this degree of overlap, thus demonstrating the significant impact of the environment. This is also graphically represented in a couple of maps in the Supporting Information (see Figure SI 4).

The two theoretical approaches yield a very significant overlap between the on-site energies for electrons in the guest and host molecules, in full consistency with the experiment. In the latter case, the activation energy (E_a) typically is roughly estimated by adding the optical gap to the ionization potential, leading to values of ∼2.2−2.9 eV for CBP[42,45] and 2.8 eV for $Ir(ppy)_3$[15]); these match the values obtained by the fragment approach fairly well.

We have computed the transfer integrals between all possible pairs of active molecules (host−host, host−guest, and guest−guest) in the pure phase and in the blend. Since no degeneracies were observed for the two frontier molecular orbitals (HOMO and LUMO), only these two levels were considered on each molecule. The corresponding distributions are displayed in Figure 5, as a function of the separation between the centers of mass. Since the magnitude of the transfer integrals reflects the degree of electronic overlap between the two orbitals, they exhibit a clear distance

DOI: 10.1021/acs.jctc.5b00057
J. Chem. Theory Comput. 2015, 11, 2077−2086

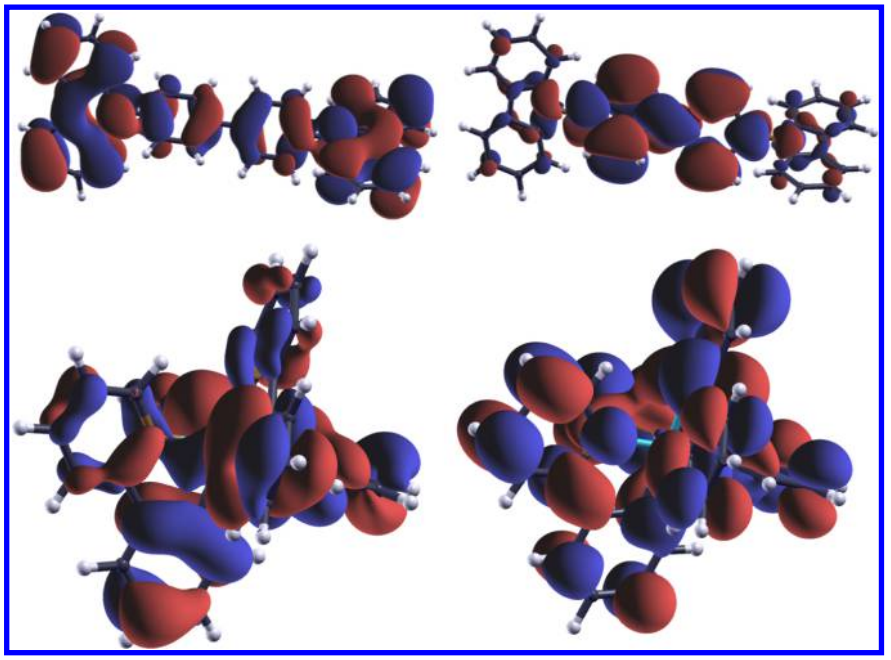

Figure 6. Shapes of the HOMO (left) and LUMO (right) orbitals for the host (top) and guest (bottom) molecules.

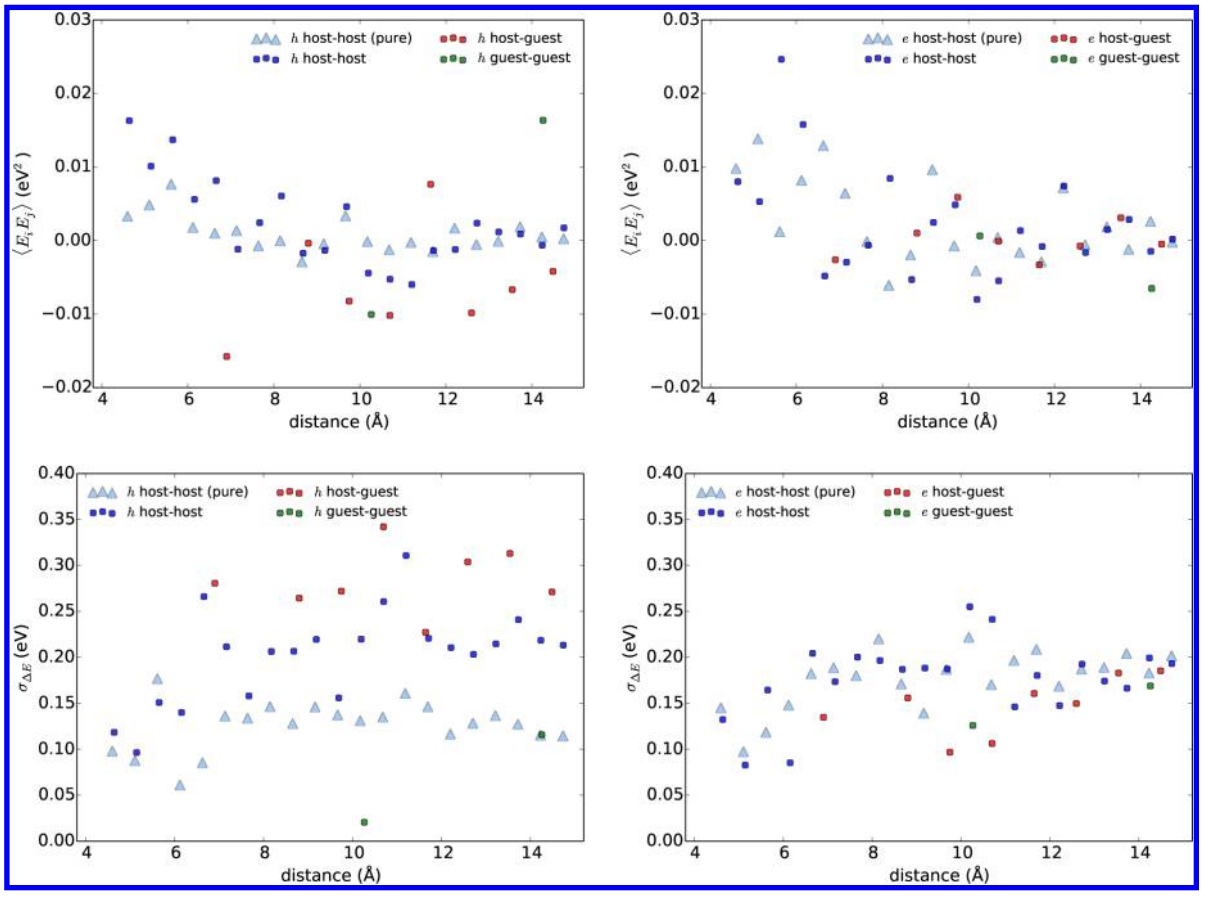

Figure 7. Correlation among CDFT site energies, associated with individual clusters. (Top) Space correlation of on-site energy differencies for holes (left) and electrons (right), in both morphologies. The quantity plotted is defined as $\langle E_i E_j \rangle = \sum_{ij}(E_i - \overline{E})(E_j - \overline{E})$, where the sum involves all pairs for which the distance $r_{ij} = |\mathbf{r}_i - \mathbf{r}_j|$ falls within an interval $[r - \delta r, r + \delta r]$; $\overline{E}$ is the average value. $\langle E_i E_j \rangle \approx 0$ corresponds to the absence of correlation. (Bottom) Evolution of the standard deviation of energy differences among sites $\sigma_{\Delta E}$ versus intermolecular distances for holes (left) and electrons (right), in both morphologies. For all plots, triangles (▲) refer to the pure host structure, while circles (●) refer to the host−guest structure.

dependence, with the largest values typically found at the shortest intermolecular interactions. Interestingly, the hole transfer integrals do not vanish at distances larger than 10 Å, in contrast to electrons (see Figure 5). This different behavior

DOI: 10.1021/acs.jctc.5b00057
J. Chem. Theory Comput. 2015, 11, 2077−2086

originates from the shape of the frontier molecular orbitals (MOs); Figure 6 shows that the LUMO of CBP is confined over the central biphenylic core, whereas the HOMO level is delocalized over the entire backbone, so that large intermolecular separations can still produce significant electronic couplings. We did find a poor correlation between the transfer integrals and the relative orientation of the molecules (see Figure S2 in the Supporting Information).

We also monitored the correlation between the on-site energies: Figure 7 shows the correlation of on-site CDFT energy differences and the corresponding standard deviation, as a function of the intermolecular separations. We observe a certain degree of correlation between on-site energies, which is weakened at distances larger than 8 Å (see Figure 7, top panels); the host−guest structure exhibits larger degrees of correlation at short distances. Such distance dependence of on-site energy correlations $\langle E_i E_j \rangle$ cannot be fitted by a simple correlated disordered model (CDM),[46] suggesting more complex contributions than a simple dipole-charge interaction. The distance-dependent character of the standard deviation of the energy differences $\sigma_{\Delta E}$ (Figure 7, bottom panels) confirms the correlated energetic order at short distances. The increase in the energetic disorder when moving from the pure host to host−guest morphology is clearly evidenced for holes (when comparing the circles versus triangles in Figure 7), as already suggested by the average σ_E in Table 1. The latter contributes to a better level alignment between host and guest molecules.

4. CONCLUSION

A fast and reliable approach has been implemented in the BigDFT code to compute key parameters for charge transport properties in large supramolecular architectures, namely, on-site energies and transfer integrals. The on-site energies have been calculated both in a one-electron picture (fragment approach) and via a constrained density functional theory (CDFT) approach, introducing a net confined charge in the system and, hence, solid-state polarization effects. The on-site energies calculated for the isolated host [guest] molecule and averaged over all clusters centered on a given host [guest] are rather similar to the two approaches in the blends, although the extent of the distribution is wider with CDFT; this indicates that CDFT is more sensitive to the details of the environment. The absolute value of the on-site energy for holes computed with CDFT agrees well with the experimental data, whereas a larger deviation is observed for the iridium complex. A larger number of virtual orbitals included in the support function optimization might help improve the values calculated for the on-site energies for electrons. The transfer integrals exhibit a distance dependence reflecting the degree of electronic delocalization of the involved orbitals; a close proximity appears to favor a better spatial correlation among the site energies for holes. The procedure described here can be repeated for other snapshots generated by the force-field calculations in order to describe the dynamical evolution of the transport parameters.

■ ASSOCIATED CONTENT

Supporting Information

Supporting Information contains further details about parameter computation. This material is available free of charge via the Internet at http://pubs.acs.org.

■ AUTHOR INFORMATION

Corresponding Authors

*E-mail: lratcliff@anl.gov (L. E. Ratcliff).
*E-mail: lgrisant@ictp.it (L. Grisanti).
*E-mail: jerome.cornil@umons.ac.be (J. Cornil).

Notes

The authors declare no competing financial interest.
[⊥]Currently at Argonne Leadership Computing Facility, Argonne National Laboratory, Argonne, IL 60439, USA.

■ ACKNOWLEDGMENTS

The work in Mons and at KIT has been supported by the European Project MMM@HPC(FP7-RI-261594), the Inter-university Attraction Pole Program of the Belgian Federal Science Policy Office (No. PAI 6/27), and the Belgian National Fund for Scientific Research (FNRS). The work in CEA has been supported by funding from the ANR projects SAMSON (No. ANR-AA08-COSI-015) and NEWCASTLE (No. ANR-2010-COSI-005-01). This research used resources of the Argonne Leadership Computing Facility at Argonne National Laboratory, which is supported by the Office of Science of the U.S. Department of Energy, under Contract No. DE-AC02-06CH11357 and Oak Ridge Leadership Computing Facility at the Oak Ridge National Laboratory, which is supported by the Office of Science of the U.S. Department of Energy, under Contract No. DE-AC05-00OR22725. Part of the calculations, including tests, were also run on HPC resources available within the MOLED project granted by European PRACE-2IP (No. FP7-RI-283493). J.C. and D.B. are FNRS research directors. T.N. thanks the BioInterfaces International Graduate School within the BioInterfaces programme at KIT, funded by the Helmholtz Association, for support and the Ministry for Science, Research and Arts Baden-Wuerttemberg (Ministerium fuer Wissenschaft, Forschung und Kunst Baden-Wuerttemberg) for funding via the Landesgraduiertenfoerderung. L.E.R. thanks Stephan Mohr for assistance with the spin-polarized calculations.

■ REFERENCES

(1) Cornil, J.; Verlaak, S.; Martinelli, N.; Mityashin, a.; Olivier, Y.; van Regemorter, T.; D'Avino, G.; Muccioli, L.; Zannoni, C.; Castet, F.; Beljonne, D.; Heremans, P. *Acc. Chem. Res.* **2013**, *46*, 434−443.
(2) Rühle, V.; Lukyanov, A.; May, F.; Schrader, M.; Vehoff, T.; Kirkpatrick, J.; Baumeier, B.; Andrienko, D. *J. Chem. Theory Comput.* **2011**, *7*, 3335−3345.
(3) Neumann, T.; Danilov, D.; Lennartz, C.; Wenzel, W. *J. Comput. Chem.* **2013**, *34*, 2716−2725.
(4) Beljonne, D.; Brocorens, P.; Cornil, J.; Lazzaroni, R.; Martinelli, N. G.; Minoia, A.; Muccioli, L.; Olivier, Y.; Ruiz-Delgado, M. C.; Zannoni, C. In *Functional Supramolecular Architectures for Organic Electronics and Nanotechnology*; F. Cacialli, P. S., Ed.; Wiley−VCH: Weinheim, Germany, 2010; pp 3−37.
(5) Ortmann, F.; Bechstedt, F.; Hannewald, K. *Phys. Status Solidi B* **2011**, *248*, 511−525.
(6) Coropceanu, V.; Cornil, J.; da Silva Filho, D. a.; Olivier, Y.; Silbey, R.; Brédas, J.-L. *Chem. Rev.* **2007**, *107*, 926−952.
(7) Troisi, A. *Chem. Soc. Rev.* **2011**, *40*, 2347−2358.
(8) Bässler, H.; Köhler, A. *Top. Curr. Chem.* **2012**, *312*, 1−66.
(9) Wu, Q.; van Voorhis, T. *J. Chem. Phys.* **2006**, *125*, 164105.
(10) Wu, Q.; van Voorhis, T. *Phys. Rev. A* **2005**, *72*, 024502.
(11) Behler, J.; Delley, B.; Reuter, K.; Scheffler, M. *Phys. Rev. B* **2007**, *75*, 115409.
(12) van Voorhis, T.; Kowalczyk, T.; Kaduk, B.; Wang, L.-P.; Cheng, C.-L.; Wu, Q. *Annu. Rev. Phys. Chem.* **2010**, *61*, 149−170.

DOI: 10.1021/acs.jctc.5b00057
J. Chem. Theory Comput. 2015, 11, 2077−2086

(13) Yeganeh, S.; Voorhis, T. V. *J. Phys. Chem. C* **2010**, *114*, 20756−20763.
(14) Castet, F.; Aurel, P.; Fritsch, A.; Ducasse, L.; Liotard, D.; Linares, M.; Cornil, J.; Beljonne, D. *Phys. Rev. B* **2008**, *77*, 1−14.
(15) Ikai, M.; Tokito, S.; Sakamoto, Y.; Suzuki, T.; Taga, Y. *Appl. Phys. Lett.* **2001**, *79*, 156.
(16) Tanaka, D.; Sasabe, H.; Li, Y.-J.; Su, S.-J.; Takeda, T.; Kido, J. *Jpn. J. Appl. Phys.* **2007**, *46*, L10−L12.
(17) Ishihara, S.; Okachi, T.; Naito, H. *Thin Solid Films* **2009**, *518*, 452−456.
(18) Helander, M. G.; Wang, Z. B.; Qiu, J.; Greiner, M. T.; Puzzo, D. P.; Liu, Z. W.; Lu, Z. H. *Science (New York, N.Y.)* **2011**, *332*, 944−947.
(19) Genovese, L.; Neelov, A.; Goedecker, S.; Deutsch, T.; Ghasemi, S. A.; Willand, A.; Caliste, D.; Zilberberg, O.; Rayson, M.; Bergman, A.; Schneider, R. *J. Chem. Phys.* **2008**, *129*, 014109.
(20) Mohr, S.; Ratcliff, L. E.; Boulanger, P.; Genovese, L.; Caliste, D.; Deutsch, T.; Goedecker, S. *J. Chem. Phys.* **2014**, *140*, 204110.
(21) Oberhofer, H.; Blumberger, J. *J. Chem. Phys.* **2010**, *133*, 244105.
(22) Senthilkumar, K.; Grozema, F. C.; Bickelhaupt, F. M.; Siebbeles, L. D. A. *J. Chem. Phys.* **2003**, *119*, 9809−9817.
(23) Senthilkumar, K.; Grozema, F. C.; Guerra, C. F.; Bickelhaupt, F. M.; Lewis, F. D.; Berlin, Y. A.; Ratner, M. A.; Siebbeles, L. D. A. *J. Am. Chem. Soc.* **2005**, *127*, 14894−14903.
(24) Ratcliff, L. E., Genovese, L., Mohr, S., Deutsch, T. J. *arXiv e-prints*. arXiv:1503.06229 [cond-mat.mtrl-sci] (accessed March 24, 2015).
(25) Sena, A. M. P.; Miyazaki, T.; Bowler, D. R. *J. Chem. Theory Comput.* **2011**, *7*, 884−889.
(26) Oberhofer, H.; Blumberger, J. *J. Chem. Phys.* **2009**, *131*, 064101.
(27) Řezáč, J.; Lévy, B.; Demachy, I.; de la Lande, A. *J. Chem. Theory Comput.* **2012**, *8*, 418−427.
(28) Souza, A. M.; Rungger, I.; Pemmaraju, C. D.; Schwingenschloegl, U.; Sanvito, S. *Phys. Rev. B* **2013**, *88*, 165112.
(29) Kaduk, B.; Kowalczyk, T.; van Voorhis, T. *Chem. Rev.* **2012**, *112*, 321−370.
(30) Wu, Q.; van Voorhis, T. *J. Chem. Theory Comput.* **2006**, *2*, 765−774.
(31) Swallen, S. F.; Kearns, K. L.; Mapes, M. K.; Kim, Y. S.; McMahon, R. J.; Ediger, M. D.; Wu, T.; Yu, L.; Satija, S. *Science* **2007**, *315*, 353−356.
(32) Kearns, K. L.; Still, T.; Fytas, G.; Ediger, M. D. *Adv. Mater.* **2010**, *22*, 39−42.
(33) Singh, S.; Ediger, M. D.; de Pablo, J. J. *Nat. Mater.* **2013**, *12*, 139−144.
(34) Metropolis, N.; Rosenbluth, A. W.; Rosenbluth, M. N.; Teller, A. H.; Teller, E. *J. Chem. Phys.* **1953**, *21*, 1087−1092.
(35) Kirkpatrick, S.; Gelatt, C. D.; Vecchi, M. P. *Science* **1983**, *220*, 671−680.
(36) Li, Z.; Scheraga, H. A. *Proc. Natl. Acad. Sci. U.S.A.* **1987**, *84*, 6611−6615.
(37) Wales, D. J.; Doye, J. P. K. *J. Phys. Chem. A* **1997**, *101*, 5111−5116.
(38) Wales, D. J.; Scheraga, H. A. *Science* **1999**, *285*, 1368−1372.
(39) Ceperley, D. M.; Alder, B. J. *Phys. Rev. Lett.* **1980**, *45*, 566−569.
(40) Hartwigsen, C.; Goedecker, S.; Hutter, J. *Phys. Rev. B* **1998**, *58*, 3641−3662.
(41) Baerends, E. J.; Ziegler, T. *ADF: SCM, Theoretical Chemistry*, Vrije Universiteit, Amsterdam, The Netherlands, 2010−2012; available via the Internet at: http://http://www.scm.com (accessed Oct. 16, 2013).
(42) Hill, I. G.; Kahn, A. *J. Appl. Phys.* **1999**, *86*, 4515.
(43) Vázquez, H.; Gao, W.; Flores, F.; Kahn, A. *Phys. Rev. B* **2005**, *71*, 041306.
(44) Dandrade, B.; Datta, S.; Forrest, S.; Djurovich, P.; Polikarpov, E.; Thompson, M. *Org. Electron.* **2005**, *6*, 11−20.
(45) Gao, W.; Kahn, A. *Appl. Phys. Lett.* **2003**, *82*, 4815.
(46) Novikov, S. V.; Dunlap, D. H.; Kenkre, V. M.; Parris, P. E.; Vannikov, A. V. *Phys. Rev. Lett.* **1998**, *81*, 4472−4475.

DOI: 10.1021/acs.jctc.5b00057
J. Chem. Theory Comput. 2015, 11, 2077−2086